

Experimental Measurements of Hot Electrons Generated by Ultraintense ($>10^{19}$ W/cm²) Laser-Plasma Interactions on Solid-Density Targets

K. B. Wharton,^{1,2} S. P. Hatchett,¹ S. C. Wilks,¹ M. H. Key,¹ J. D. Moody,¹ V. Yanovsky,¹ A. A. Offenberger,³
B. A. Hammel,¹ M. D. Perry,¹ and C. Joshi²

¹*Lawrence Livermore National Laboratory, University of California, P.O. Box 808, Livermore, California 94550*

²*Department of Electrical Engineering, University of California, Los Angeles, California 90024*

³*Department of Electrical Engineering, University of Alberta, Edmonton, Alberta, Canada T6G 2G7*

(Received 8 December 1997)

We present the first in-target measurements of the electrons produced by an ultraintense ($I > 10^{19}$ W/cm²) laser pulse incident on a massive solid target. Total conversion efficiency, mean electron energy, and electron cone-angle measurements are presented. A relationship between the target material and the mean electron energy is also discussed. [S0031-9007(98)06709-X]

PACS numbers: 52.40.Nk, 52.50.Jm, 52.58.Ns

Experimental investigation of plasma phenomena in ultraintense laser fields, in which electrons oscillate at relativistic velocities, has recently become possible with the advent of multiterawatt, short-pulse lasers. Several mechanisms have been described which can transfer laser energy to the plasma electrons [1]. One proposed application for these energetic electrons is sparking a fusion reaction in the fast ignitor scheme [2]. Crucial but unresolved issues include the conversion efficiency of laser energy to electron energy, the electron directionality, and the temperature or mean energy of the electrons. In this Letter we present the first measurements of the laser-to-electron conversion efficiency, directionality, and mean electron energy in laser-solid interactions at incident laser intensities of $(2-4) \times 10^{19}$ W cm⁻².

One mechanism for collisionless laser-electron coupling in a plasma is the $-e\mathbf{v} \times \mathbf{B}$ Lorentz force on electrons oscillating in the electromagnetic field of a high-intensity laser. When the laser fields terminate at a critical-density surface, this force can ponderomotively accelerate electrons in the direction of laser propagation [3]. Other collisionless laser-electron coupling mechanisms at the critical density include resonance absorption [4], parametric instabilities [5], and vacuum heating [6]. Coupling at subcritical densities associated with the excitation of electron plasma waves can also accelerate plasma electrons [7]. Previous experiments have measured laser-accelerated electrons at lower intensities [8-14]. One recent experiment using strongly relativistic intensities ($I\lambda^2 > 10^{19}$ W cm⁻² μm²) measured high-energy electrons in vacuum after leaving a foil target in which they were produced [15].

Our experiments were performed at the Nova laser facility at LLNL, on a beam line which utilizes chirped pulse amplification [16]. This short-pulse system supplies 12-30 J of 1.06 μm light in 400 fs. The peak intensity is 10⁷ times greater than the amplified spontaneous emission (ASE), which begins about 3 ns before the main pulse. An additional 400 fs prepulse, reaching $\sim 10^{-3}$ of the peak in-

tensity, arrives ~ 2 ns early. The final focusing optic is an $f/3$ off-axis parabola, which produces a measured 15 μm FWHM focal spot (peak intensity of 4×10^{19} W cm⁻² for 30 J). Measurements [17] and simulations show that the ASE and prepulse create an underdense plasma in front of the target with a scale length on the order of 10 μm. In this plasma the intense laser may experience filamentation and self-focusing [18,19], which have been seen to raise the peak laser intensity by a factor of ~ 4 in comparable 2D simulations [1].

Both the temperature and the absolute number of the laser-produced electrons were characterized by detecting the electron-induced K_α x-ray emission from buried layers in multilayer targets, a well-established technique [8-12,14]. This is an indirect method for measuring the electrons before they leave the target via the inner-shell ionization of a tracer material at a known depth in the target. By varying the depth of the tracer layer, an electron spectrum can be inferred from the corresponding change in the K_α x-ray yield.

In the experiment the p -polarized laser light was incident at 25° to the target normal. The front (laser-incident) layer of the target was a 6 mm by 8 mm rectangular foil of various materials (CH, Al, or Cu) with a mass per unit area ranging from 0.02 to 0.45 g/cm². The middle layer of the target was a smaller foil (5 mm by 7 mm) of 50-μm-thick molybdenum. Electrons produced in the front layer move into this Mo layer, knocking out inner-shell electrons and creating 17.5 keV K_α x rays. Finally, a layer of 1 mm thick CH (6 mm by 8 mm) covered the back of the target, which protected the Mo layer from electrons that might return to the target (pulled back by electrostatic forces). This CH layer stopped electrons with energies below 300 keV (550 keV for a double pass), while having a negligible effect on the 17.5 keV x rays. We found that this layer lowered the Mo K_α x-ray signal by a factor of ~ 2 , which indicated that most of the K_α radiation was produced by electrons, and not photopumped by x rays.

We chose Mo for our tracer material so that the characteristic 17.5 keV K_α photon energy would be significantly greater than that of the x rays produced by the thermal plasma around the laser focus. This is important to avoid photopumping of the K_α x-ray line [8]. Spectroscopic measurements of an Al layer buried under a very thin layer of 5 μm CH showed a thermal plasma temperature of 300–600 eV in separate experiments with the same laser [20]. Further evidence that thermal x rays were unimportant was that the 20–30 keV x-ray spectrum was very similar from both the front and back of pure Al and Cu targets which were optically thick in this energy range. This signified that these x rays were predominantly bremsstrahlung photons produced throughout the cold target.

K_α x rays from the Mo layer were detected by a 16-bit charged-coupled device (CCD) detector, situated 2.16 m from the target and 45° from the rear target normal. The CCD was filtered with 75 μm of Sn, limiting the x-ray flux and making it unlikely that two high-energy photons would be absorbed in the same pixel. The counts recorded on each pixel were proportional to the x-ray photon energy. A statistical analysis was performed on each set of data to determine what fraction of the signal was obscured by double hits due to the lower energy x-ray continuum.

The CCD camera was absolutely calibrated with a Cd-109 (22 keV) source at two different occasions during the experiments. The two calibrations agreed to within 3% and allowed us to calculate the number of incident x rays from the measured hits on the camera. To scale the 22 keV calibration energy to the 17.5 keV K_α x rays, we assumed the detector response was proportional to the absorption of the 14 μm thick Si CCD chip.

The many possible electron trajectories in the target made a comprehensive analytical description difficult. Instead we used the electron-photon transport Monte Carlo code ITS [21] to interpret the data. The output of this code was the number of K_α x rays per steradian emitted from a given target in the detector direction, normalized to the number of source electrons. In addition to calculating the electron transport and ionization, ITS also computed the x-ray continuum produced by bremsstrahlung of the fast electrons and the resulting photoionization of the Mo atoms. The photopumped K_α x rays were typically 10% of the total.

We assumed that the electron source has the form of a Maxwellian energy distribution, which has been seen in PIC simulations [3,19] and in experiments [11,15]. However, as there is no intrinsic reason why the electrons should be Maxwellian, we also ran ITS simulations of other possible distributions. For a relativistic Maxwellian, the mean electron energy E_0 ranges from $\frac{3}{2}kT$ (nonrelativistic electrons) to $3kT$ (highly relativistic electrons). We compared this to the case of a purely exponential spectrum $f(E) = \exp(-E/kT)$, for which $E_0 = kT$. The ITS results were entirely consistent to within 10% for these different spectra, provided that E_0 (not kT) was

kept constant. This demonstrates that our technique is not sensitive to the tail of the electron distribution (the slope of which determines kT), but rather to the mean-energy bulk of the distribution. For this reason, our results are not directly comparable to some previous measurements of bremsstrahlung x rays or the high-energy electron tail [15]. However, our technique is appropriate for absolute conversion efficiency measurements which depend on the mean-energy E_0 .

One assumption required in ITS is the cone-angle of the electrons. For now we assume that the electrons spray forward isotropically from the laser focus into a full hemisphere; we discuss this further below. ITS also assumes that the electrons propagate through cold material, and the code ignores collective effects such as self-consistent magnetic [19,22] and electrostatic fields [23–25]. Because of the complexity of the physics involved, our use of ITS is not intended to fully model the experiment but is used as a benchmark for interpreting the data.

The Mo K_α yields from the targets with aluminum front layers are presented in Fig. 1, along with the best fits from the ITS code. The slope of the data (on a log plot) is sensitive to the mean-energy E_0 of the electrons, while the absolute magnitude yields the laser-to-electron conversion efficiency η . Error bars were computed from a combination of counting errors and fluctuations in the background x-ray noise.

We fitted the data with a series of ITS runs which computed the K_α x-ray yield as a function of the transport layer thickness for a given electron mean-energy E_0 , and then found the conversion efficiency η which minimized the chi-squared per degree of freedom. The data at an

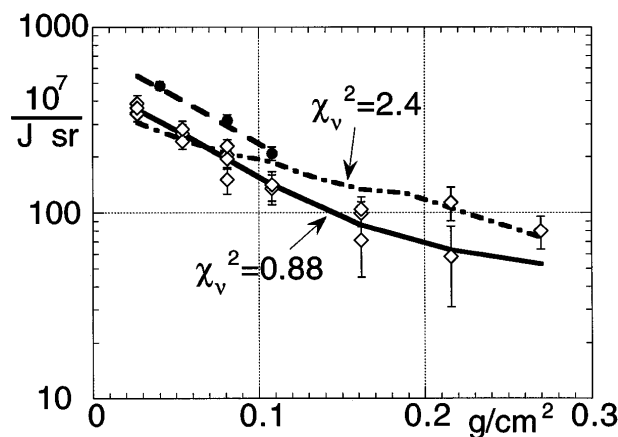


FIG. 1. K_α signal from the Al targets, in units of 10^7 x rays per incident joule and per steradian, plotted against areal mass of the aluminum front layer of the target. The solid circles are experimental data at intensities of $4 \times 10^{19} \text{ W cm}^{-2}$, empty diamonds are data at $2 \times 10^{19} \text{ W cm}^{-2}$. The solid line is an ITS fit with mean-energy $E_0 = 330 \text{ keV}$ and conversion efficiency $\eta = 31\%$. The dash-dotted line is $E_0 = 640 \text{ keV}$ and $\eta = 30\%$. The dashed line is $E_0 = 330 \text{ keV}$ and $\eta = 47\%$. All values of η are multiplied by 0.7 if the electrons are assumed to be directed in a 30° half-angle cone.

intensity of $2 \times 10^{19} \text{ W cm}^{-2}$ are fitted by an ITS run with $E_0 = 330 \text{ keV}$ ($kT = 170 \text{ keV}$) and $\eta = 31\%$. For this fit, the chi-squared is reasonably small (0.88). An ITS run for $E_0 = 640 \text{ keV}$ ($kT = 300 \text{ keV}$) is also shown, although the chi-squared of this fit is much larger (2.4). Three data points at an intensity of $4 \times 10^{19} \text{ W cm}^{-2}$ show a higher η (47%) but roughly the same mean energy.

Figure 2 shows the experimental results for CH and Cu targets at a laser intensity of $2 \times 10^{19} \text{ W cm}^{-2}$. The CH targets produced the smallest signal, corresponding to $E_0 = 120 \text{ keV}$ and $\eta = 29\%$. The Cu data have the largest error bars, due to higher x-ray noise, but are best fitted by $E_0 = 640 \text{ keV}$ and $\eta = 29\%$. Higher and lower energy fits to the Cu data are shown as well. The lower-intensity Al data from Fig. 1 are at the same intensity; recall they were fitted by $E_0 = 330 \text{ keV}$ and $\eta = 31\%$. The data show a change of mean electron energy with target material, although the conversion efficiencies remain roughly constant.

The assumption that the electrons are spraying into a full hemisphere might artificially increase the apparent conversion efficiency. To measure the directionality of the electrons, a stainless steel razor blade of $750 \mu\text{m}$ thickness was placed between the back of the target and the CCD detector, creating a 1D penumbral image of the x-ray source on the CCD [11,26]. Using this configuration, $2 \times 10^{19} \text{ W cm}^{-2}$ laser pulses were shot at some of the previously described targets; CH front layers (varied thicknesses), Mo middle layers, and optional CH back layers to prevent electron double hits. The lack of

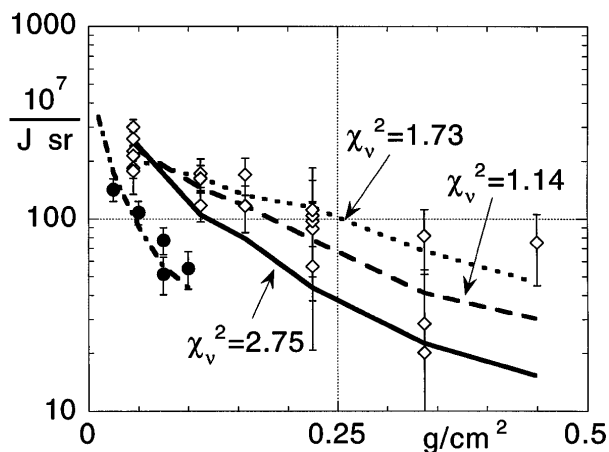


FIG. 2. K_{α} signal from the target, the same units as Fig. 1. The solid circles are data from CH front-layer targets, and empty diamonds are data from Cu targets, both at $2 \times 10^{19} \text{ W cm}^{-2}$. The solid line is an ITS fit in Cu with mean-energy $E_0 = 330 \text{ keV}$ and conversion efficiency $\eta = 30\%$. The dashed line is $E_0 = 640 \text{ keV}$ and $\eta = 29\%$. The dotted line is $E_0 = 1040 \text{ keV}$ and $\eta = 31\%$. The dash-dotted line is an ITS fit in CH for $E_0 = 120 \text{ keV}$ and $\eta = 29\%$. All values of η are multiplied by 0.7 if the electrons are assumed to be directed in a 30° half-angle cone.

measured x rays above 6 keV from pure CH targets, along with the opacity of the razor blade to x rays under 25 keV , meant that the size of the $6\text{--}25 \text{ keV}$ x-ray source was a good measure of where the electron beam intersected the Mo layer. Varying the depth of the Mo gave us an estimate of the electron cone-angle.

Figure 3 shows this measured spot size graphed against the buried depth of the $50 \mu\text{m}$ Mo layer, and compares it to ITS calculations of the predicted measurements for electron beams with 30° and 90° half-cone angles. The large error bars result from the derivative that is required to extract the spot size from the data. For Mo layers buried 100 to $250 \mu\text{m}$ into the target, the data roughly correspond to an electron cone half-angle of 90° , a full hemisphere. However, for the thicker targets the x-ray source corresponds closer to an electron beam of a 30° half-cone angle. Although the error bars are large, these data suggest some beaming of the high-energy electrons ($>200 \text{ keV}$) that penetrate through the thicker targets. The bulk of the lower-energy electrons seem to be spraying into a full hemisphere. Although the high-energy cone-angle is essentially unknown, using ITS to recalculate the conversion efficiencies based on a 30° half-angle electron source lowers η to 0.7 of the above-quoted 90° values. The mean electron energies were not affected.

Applying this beaming effect to the earlier data, our measurements correspond to $\eta = 21\% \pm 5\%$ for all materials at a laser intensity of $2 \times 10^{19} \text{ W cm}^{-2}$, and $\eta = 33\% \pm 5\%$ for the high-intensity ($4 \times 10^{19} \text{ W cm}^{-2}$) shots on Al targets.

The average-energy measurements, however, vary with target material rather than intensity. Our data show that the Cu-produced electrons are the most penetrating, although the error bars on the measurements still allow the possibility that the Al and Cu spectra could be equivalent.

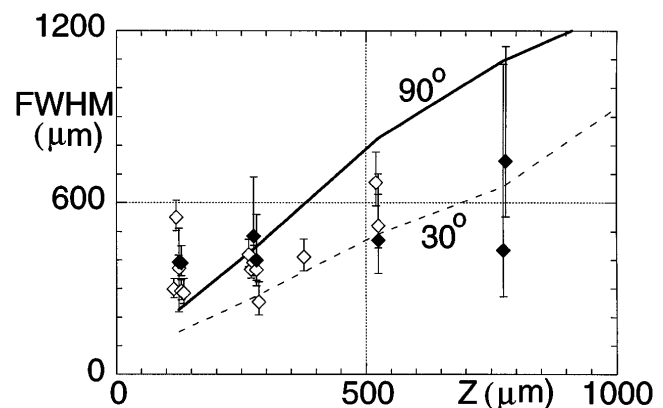


FIG. 3. The measured size (FWHM in μm) of the x-ray source is plotted against thickness of the front CH layer in μm . Solid diamonds are from targets with a back layer of 1 mm CH; empty diamonds had no back CH layer. The solid line is an ITS fit of the expected results from an unbeamed electron source (90° half-angle). The dashed line is an ITS simulation of an electron source with a 30° half-angle.

The CH electrons are less penetrating and apparently colder, although they seem to have roughly the same conversion efficiency as the Al and Cu targets. The conversion efficiency in CH, however, has an additional systematic error because the range of an $E_0 = 120$ keV electron is smaller than the typical target thickness, which means that in CH we are not measuring the bulk of the electron distribution as we do in Al and Cu.

Bell, Davies, and collaborators have pointed out that strong material-dependent effects may result from differences in target conductivity [24,25]. Conductivity has long been known to play an important role in shielding the resistive electrostatic field via a return current [23]. In our experiment the return current also serves as the primary source of the hot electrons, because the number of fast electrons we infer from our experiment is much greater than the number of electrons in a cubic laser spot size.

We have performed 1D LASNEX [27] simulations in which a high-energy Maxwellian distribution of electrons propagates from the center of a solid density sphere. The return current, heating, conductivity, and electrostatic fields are calculated self-consistently, and show a $\sim 40\%$ loss of electron energy to resistive electrostatic fields. Other simulations have put this number at 30% [25]. This loss implies that our measurements of the fast electrons must be lower bounds on the original electron parameters, ideally requiring a correction for electrostatic effects.

However, electrostatic effects cannot fully explain the observed material dependence because η is not lowered by the same factor as E_0 in the different target materials. Another difference between the target materials is the underdense plasma that the ASE and prepulse form in front of the target. 2D calculations with LASNEX show a larger separation between the regions of critical and solid densities in CH ($40 \mu\text{m}$), compared to Al ($22 \mu\text{m}$) and Cu ($18 \mu\text{m}$). This difference is due to the variation in the Z of the target, and it will affect the intensity distribution of the laser through filamentation instabilities and relativistic self-focusing [18,19].

In summary, we have demonstrated a 20%–30% conversion efficiency from laser energy into forward-propagated electrons in solid targets. This efficiency seems to be a function of intensity but not target material. A material dependence on electron temperature has been demonstrated for the first time at intensities above $10^{19} \text{ W cm}^{-2}$.

The authors thank C. Brown, Y. Zakharenkov, J. Koch, and D. Pennington for their valuable contributions and

support. This work was performed under the auspices of the U.S. Department of Energy by Lawrence Livermore National Laboratory under Contract No. W-7405-ENG-48.

-
- [1] S. C. Wilks and W. L. Kruer, IEEE J. Quantum Electron. **33**, 1954 (1997).
 - [2] M. Tabak *et al.*, Phys. Plasmas **1**, 1626 (1994).
 - [3] S. C. Wilks *et al.*, Phys. Rev. Lett. **69**, 1383 (1992).
 - [4] N. H. Ebrahim *et al.*, Phys. Rev. Lett. **45**, 1179 (1980); F. Brunel, Phys. Rev. Lett. **59**, 52 (1987).
 - [5] K. Estabrook and W. L. Kruer, Phys. Fluids **26**, 7 (1983).
 - [6] F. Brunel, Phys. Rev. Lett. **59**, 52 (1987).
 - [7] D. W. Forslund *et al.*, Phys. Rev. A **11**, 670 (1975); G. J. Pert, Plasma Phys. **20**, 175 (1978); M. J. Everett *et al.*, Nature (London) **368**, 527 (1994); A. Modena *et al.*, Nature (London) **377**, 606 (1995).
 - [8] J. D. Hares *et al.*, Phys. Rev. Lett. **42**, 1216 (1979).
 - [9] N. A. Ebrahim, C. Joshi, and H. A. Baldiss, Phys. Rev. A **25**, 2440 (1982); B. Luther-Davies, A. Perry, and K. A. Nugent, Phys. Rev. A **35**, 4306 (1987).
 - [10] H. Chen *et al.*, Phys. Rev. Lett. **70**, 3431 (1993).
 - [11] A. Rousse *et al.*, Phys. Rev. E **50**, 2200 (1994).
 - [12] Z. Jiang *et al.*, Phys. Plasmas **2**, 1702 (1995).
 - [13] U. Teubner *et al.*, Phys. Rev. E **54**, 4167 (1996).
 - [14] F. N. Beg *et al.*, Phys. Plasmas **4**, 447 (1997).
 - [15] G. Malka and J. L. Miquel, Phys. Rev. Lett. **77**, 75 (1996).
 - [16] B. C. Stuart *et al.*, Opt. Lett. **22**, 242 (1997).
 - [17] Y. Zakharenkov *et al.*, Rev. Sci. Instrum. **68**, 847 (1997).
 - [18] C. E. Max *et al.*, Phys. Rev. Lett. **33**, 209 (1974); P. Sprangle *et al.*, IEEE Trans. Plasma Sci. **PS-15**, 145 (1987); W. B. Mori *et al.*, Phys. Rev. Lett. **60**, 1298 (1988).
 - [19] A. Puhkov and J. Meyer-ter-Vehn, Phys. Rev. Lett. **76**, 3975 (1996).
 - [20] J. Koch *et al.*, Laser Part. Beams **16**, 225 (1998).
 - [21] J. A. Halbleib and T. A. Mehlhorn, Nucl. Sci. Eng. **92**, 338 (1986).
 - [22] M. G. Haines, Phys. Rev. Lett. **78**, 254 (1997).
 - [23] D. J. Bond, J. D. Hares, and J. D. Kilkenny, Phys. Rev. Lett. **45**, 252 (1980).
 - [24] A. R. Bell *et al.*, Plasma Phys. Controlled Fusion **39**, 653 (1997).
 - [25] J. R. Davies *et al.*, Phys. Rev. E **56**, 7193 (1997).
 - [26] A. P. Fews *et al.*, Opt. Commun. **94**, 259 (1992).
 - [27] G. B. Zimmerman and W. L. Kruer, Comments Plasma Phys. Control. Fusion **2**, 85 (1975).